Supporting Information

From order to disorder: Computational design of triblock amphiphiles with 1-nm domains

Zhengyuan Shen,[a,b] Jingyi L. Chen,[b,c] Viktoriia Vernadskaia,[b,#] S. Piril Ertem,[c] Mahesh K. Mahanthappa,[a] Marc A. Hillmyer,[c] Theresa M. Reineke,[c] Timothy P. Lodge[a,c*] and J. Ilja Siepmann[a,b,c*]

(a) Department of Chemical Engineering and Materials Science, University of Minnesota, 421 Washington Avenue SE, Minneapolis, Minnesota 55455-0132, United States

(b) Chemical Theory Center, University of Minnesota, 207 Pleasant St. SE, Minneapolis, Minnesota 55455-0431, United States

(c) Department of Chemistry, University of Minnesota, 207 Pleasant St. SE, Minneapolis, Minnesota 55455-0431, United States

(#) Current address: Laboratory of Solution Chemistry of Advanced Materials and Technologies, ITMO University, 9 Lomonosova St, Saint Petersburg, Russian Federation

(*) Corresponding authors' e-mail: lodge@umn.edu, siepmann@umn.edu

Additional Details on the Force Field and Calculation of Structure Factors

The parameters for non-bonded Lennard-Jones (LJ) and Coulomb interactions taken from the TraPPE-UA force field[1–4] are listed in **Table S1**. Here, CH_q groups are presented as pseudo-atoms, whereas the polar hydrogen belonging to a hydroxyl group is modelled explicitly, but does not carry a LJ site.

A short-range repulsive potential is applied for 1-5 interactions between hydrogen and oxygen atoms in hydroxyl groups that are separated by four bonds, to control the strength of the intramolecular H-bond for neighboring hydroxyl groups that do not involve a 1-4 O-O LJ interaction but a 1-4 Coulomb interactions scaled by a factor of 0.5.[3] The repulsive potential $U_{\text{repulsive}}(r_{ij})$ is as follows:

$$U_{\text{repulsive}}(r_{ij})/k_{\text{B}} = \frac{7.5 \times 10^{7}\,\text{K} \cdot \text{Å}^{12}}{r_{ij}^{12}} \tag{S1}$$

where r_{ij} is the 1-5 distance between hydrogen and oxygen atoms.

The other bonded interactions include bond stretching, angle bending, and torsional potentials. The corresponding interaction parameters are listed in **Table S2**, and the following functional forms are implemented to calculate the potentials:

$$u_{\text{stretching}}(r) = \frac{k_{\text{s}}}{2}(r - r_0)^2 \tag{S2}$$

$$u_{\text{bending}}(\theta) = \frac{k_{\text{b}}}{2}(\theta - \theta_0)^2 \tag{S3}$$

$$u_{\text{torsion}}(\phi) = c_0 + c_1[1 + \cos(\phi)] + c_2[1 - \cos(2\phi)] + c_3[1 + \cos(3\phi)] \tag{S4}$$

In the standard TraPPE-UA force field used for Monte Carlo simulations, the bond lengths are fixed. In modern MD algorithms, this choice is computationally inefficient. Therefore, the bonds are allowed to stretch in MD, where the bond stretching force constants are taken from the OPLS force field.[5] The p-LINCS algorithm was used to constrain the O−H bond length, which allowed for the use of the larger time step.[6] The parameters for bending and torsional potentials are taken from the TraPPE-UA force field.[1–4]

The structure factor $S(\mathbf{q})$ was calculated by:

$$S(\mathbf{q}) = \frac{\left(\sum_{j}^{N_{\text{site}}} f_j(\mathbf{q}) \cos\left(\mathbf{q} \cdot \boldsymbol{r}_j\right)\right)^2 + \left(\sum_{j}^{N_{\text{site}}} f_j(\mathbf{q}) \sin\left(\mathbf{q} \cdot \boldsymbol{r}_j\right)\right)^2}{\sum_{j}^{N_{\text{site}}} f_j^2(\mathbf{q})} \tag{S5}$$

where $\mathbf{q}$ is the scattering wave vector, $\boldsymbol{r}_j$ is the position vector of the interaction site j, N_{site} is the number of interaction sites in the simulation box, and $f_j(\mathbf{q})$ is the atomic form factor as a function of the magnitude of $\mathbf{q}$. For CH_q pseudo-atoms, the atomic form factor for carbon is used, whereas the atomic form factors for oxygen and hydrogen are used for the hydroxy oxygen and hydrogen, respectively. All the functional forms of the atomic form factors are taken from the International Tables for Crystallography.[7] The possible wave vectors included by the simulation box were computed using the following relationship:

$$\mathbf{q} = \frac{2\pi}{L_x} n_x \boldsymbol{e_x} + \frac{2\pi}{L_y} n_y \boldsymbol{e_y} + \frac{2\pi}{L_z} n_z \boldsymbol{e_z} \tag{S6}$$

where L_x, L_y, and L_z are the lengths of the simulation box in x, y, and z direction, with $\boldsymbol{e}_x$, $\boldsymbol{e}_y$, and $\boldsymbol{e}_z$ being unit basis vectors in these directions (i.e. $\boldsymbol{e}_x$ = [1 0 0] in the orthorhombic system). The reported $S(q)$ data were obtained by taking the average values of $S(\mathbf{q})$ with the same magnitude of the wave vector, $|\mathbf{q}|$. Uncertainties of $S(\mathbf{q})$ are reported as 95% confidence interval.

Supplementary Tables

Table S1. Non-bonded Lennard-Jones parameters and partial charges[1–4] for the interaction sites (pseudo-atoms) highlighted in bold.

interaction site	σ [Å]	ε/k_B [K]	q [|e|]
$\mathbf{CH_3}$	3.75	98	0
CH_x-**$\mathbf{CH_2}$-**CH_x	3.95	46	0
CH_x -**$\mathbf{CH_2}$**-O-H	3.95	46	0.265
$(CH_x)_2$-**CH-**O-H	4.33	10	0.265
O	3.02	93	–0.700
H	N/A	N/A	0.435

Table S2. Bonded interaction parameters.[1–5]

stretching	r_0 [Å]	$k_\mathrm{s}/k_\mathrm{B}$ [K]		
CH_x–CH_y	1.54	270000		
CH_x–O	1.43	322000		
O-H	0.945	constrained		
bending	ϕ_0 [°]	$k_\mathrm{b}/k_\mathrm{B}$ [K]		
CH_x–(CH_2)-CH_y	114	62500		
CH_x–(CH)-CH_y	112	62500		
CH_x–(O)-H	108.5	55400		
CH_x–(CH)-O	109.5	50400		
torsion	c_0/k_B [K]	c_1/k_B [K]	c_2/k_B [K]	c_3/k_B [K]
-CH_2-CH_2-	0.0	355.03	–68.19	791.32
-CH_x-CH-	–251.06	428.73	–111.85	441.27
CH_x-CH_2-O-H	0.0	209.82	–29.17	187.93
CH_x-CH-O-H	215.89	197.33	31.46	–173.92

Table S3. Lengths of simulation trajectories (μs) and number of molecules in all systems.

T_{SIM} [K]	ABA									BAB		AB			
	$A_2B_2A_2$	$A_2B_4A_2$	$A_2B_5A_2$	$A_2B_6A_2$	$A_2B_7A_2$	$A_2B_8A_2$	$A_2B_{10}A_2$	$A_2B_{12}A_2$	$A_3B_{12}A_3$	$B_6A_4B_6$	$B_6A_6B_6$	A_2B_6	A_3B_6	A_4B_{12}	A_6B_{12}
340	2.2 1000	2.0 1000	9.6 1000	2.3 1000	3.0 1000	2.0 1000						1.0 1000			
370	1.8 1000	1.6 1000	10.0 1000	3.2 1000	3.0 1000	2.0 1000	2.0 1000	3.2 1000				1.0 1000	1.2 1000		
400		1.6 1000	10.5 1000	3.0 1000	3.0 1000	2.0 1000	2.0 1000	3.1 1000				1.0 1000	1.2 1000		
430				3.0 1000	3.0 1000	2.0 1000	2.0 1000	3.1 1000	2.0 1000	4.5 1504		1.0 1000	1.2 1000		
440										4.3 1504					
460				2.0 1000	1.4 1000	1.2 1000	2.0 1000	1.9 2000	2.3 1000	4.7 1504			1.2 1000	1.8 1000	
490								2.8 1000	2.2 2000	3.0 1504	2.2 1000		1.2 1000	1.3 1000	1.9 1000
520								3.2 1000	2.6 1000	2.2 1504	2.2 1000			1.2 1000	2.2 1000
550									2.5 1000		2.2 1000			1.3 1000	1.3 1000
580											2.2 1000			1.5 1000	2.1 1000
610											2.2 1000				1.7 1000
640															1.2 1000
670															1.1 1000

Table S4. Lengths of simulation trajectories (μs) and number of molecules in $A_1B_yA_1$ triblock, triblock/pentablock, and disperse triblock systems.

T_{SIM} [K]	$A_1B_yA_1$	ABA/ABAABA	$ABA_{disperse}$	$BAB_{disperse}$
	$A_1B_{12}A_1$	$A_2B_{12}A_2/A_2B_{12}A_4B_{12}A_2$	$A_3B_{10}A_3/A_3B_{12}A_3/A_3B_{14}A_3$	$B_5A_6B_5/B_6A_6B_6/B_7A_6B_7$
400	1.2 1000			
430	1.2 1000	2.0 980/20		
460	1.2 1000			
490			1.6 1.6 1.6 100/800/100 250/500/250 500/0/500	
520				2.0 2.0 2.0 100/800/100 250/500/250 500/0/500

Table S5. Average number of intermolecular H-bonds per hydroxyl group for all oligomers. Data for ordered morphologies are highlighted in bold font.

T_{SIM} [K]	ABA									BAB		AB			
	$A_2B_2A_2$	$A_2B_4A_2$	$A_2B_5A_2$	$A_2B_6A_2$	$A_2B_7A_2$	$A_2B_8A_2$	$A_2B_{10}A_2$	$A_2B_{12}A_2$	$A_3B_{12}A_3$	$B_6A_4B_6$	$B_6A_6B_6$	A_2B_6	A_3B_6	A_4B_{12}	A_6B_{12}
340	1.06	1.06	1.06	1.05	1.06							1.11			
370	1.02	1.00	1.00	**1.03**	**1.05**	1.03	1.02	1.09				1.02	0.90		
400		0.96	0.94	**1.00**	**1.00**	**1.00**	**0.99**	**1.09**				0.92	**0.88**		
430				**0.94**	**0.93**	**0.94**	**0.94**	**1.00**	0.81	0.83		0.79	**0.88**		
440										**0.83**					
460				0.82	0.79	0.79	0.81	**0.92**	**0.81**	0.79			0.75	0.71	
490								0.74	**0.76**	0.71	0.80		0.68	**0.77**	0.81
520								0.65	**0.70**	0.64	**0.74**			**0.71**	**0.75**
550									0.58		**0.68**			0.64	**0.70**
580											**0.61**			0.55	**0.66**
610											0.52				**0.61**
640															**0.59**
670															0.52

Table S6. Molar volumes [cm^3/mol] of triblock and diblock amphiphiles at various simulation temperatures Data for ordered morphologies are highlighted in bold font.

T_{SIM} [K]	ABA									BAB		AB			
	$A_2B_2A_2$	$A_2B_4A_2$	$A_2B_5A_2$	$A_2B_6A_2$	$A_2B_7A_2$	$A_2B_8A_2$	$A_2B_{10}A_2$	$A_2B_{12}A_2$	$A_3B_{12}A_3$	$B_6A_4B_6$	$B_6A_6B_6$	A_2B_6	A_3B_6	A_4B_{12}	A_6B_{12}
340	119.7_4	153.3_8	170.6_7	187.8_6	203.4_4							163.5_3			
370	121.0_7	155.9_7	173_1	$\mathbf{188_1}$	$\mathbf{203.2_6}$	221.2_5	256_1	286.9_7				167.9_2	182.1_7		
400		158.4_7	176.8_6	$\mathbf{188.6_6}$	$\mathbf{206.0_3}$	$\mathbf{221.6_8}$	$\mathbf{256.0_3}$	$\mathbf{287_1}$				171.2_1	$\mathbf{185.0_4}$		
430				$\mathbf{191.9_7}$	$\mathbf{209.9_4}$	$\mathbf{226.0_6}$	$\mathbf{259.8_7}$	$\mathbf{286.7_3}$	339_1	319_1		176.0_1	$\mathbf{189.1_4}$		
440										$\mathbf{318.7_7}$					
460				202_1	222.1_3	240.7_3	275.7_5	$\mathbf{294.0_4}$	$\mathbf{344.2_4}$	325_1			196.8_2	335_1	
490								316.7_5	$\mathbf{350.0_3}$	337.2_6	337.4_9		202.9_2	$\mathbf{335.3_4}$	358_1
520								325.5_2	$\mathbf{356.4_9}$	347.7_5	$\mathbf{348_1}$			$\mathbf{336_1}$	$\mathbf{371_1}$
550									373.1_3		$\mathbf{365_1}$			348_1	$\mathbf{378_1}$
580											$\mathbf{381_1}$			364.2_7	$\mathbf{386.7_8}$
610											401_1				$\mathbf{395.3_8}$
640															$\mathbf{404.3_2}$
670															426.1_5

Table S7. Fraction and type of intermolecular hydrogen bonds between each pair of hydroxy oxygens for $A_2B_6A_2$ at T_{SIM} = 430 K.

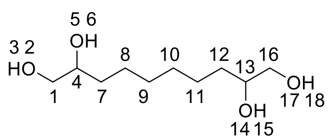

O_i	O_j	fraction	H-bond type
2	2	0.066	pri-pri
2	5	0.065	pri-sec
2	14	0.068	pri-sec
2	17	0.069	pri-pri
5	2	0.066	pri-sec
5	5	0.048	sec-sec
5	14	0.050	sec-sec
5	17	0.069	pri-sec
14	2	0.069	pri-sec
14	5	0.049	sec-sec
14	14	0.048	sec-sec
14	17	0.066	pri-sec
17	2	0.068	pri-pri
17	5	0.067	pri-sec
17	14	0.065	pri-sec
17	17	0.066	pri-pri

Table S8. Fraction and type of intermolecular hydrogen bonds between each pair of hydroxy oxygens for $A_2B_8A_2$ at T_{SIM} = 430 K.

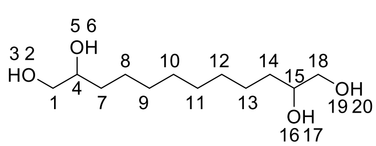

O_i	O_j	fraction	H-bond type
2	2	0.067	pri-pri
2	5	0.066	pri-sec
2	16	0.066	pri-sec
2	19	0.067	pri-pri
5	2	0.067	pri-sec
5	5	0.049	sec-sec
5	16	0.048	sec-sec
5	19	0.066	pri-sec
16	2	0.067	pri-sec
16	5	0.049	sec-sec
16	16	0.050	sec-sec
16	19	0.067	pri-sec
19	2	0.068	pri-pri
19	5	0.068	pri-sec
19	16	0.067	pri-sec
19	19	0.067	pri-pri

Table S9. Fraction and type of intermolecular hydrogen bonds between each pair of hydroxy oxygens for $A_2B_{10}A_2$ at T_{SIM} = 430 K.

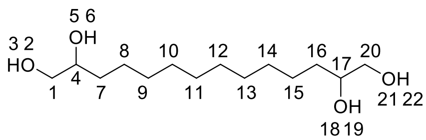

O_i	O_j	fraction	H-bond type
2	2	0.067	pri-pri
2	5	0.066	pri-sec
2	18	0.066	pri-sec
2	21	0.067	pri-pri
5	2	0.066	pri-sec
5	5	0.050	sec-sec
5	18	0.049	sec-sec
5	21	0.066	pri-sec
18	2	0.068	pri-sec
18	5	0.050	sec-sec
18	18	0.050	sec-sec
18	21	0.067	pri-sec
21	2	0.068	pri-pri
21	5	0.067	pri-sec
21	18	0.066	pri-sec
21	21	0.066	pri-pri

Table S10. Fraction and type of intermolecular hydrogen bonds between each pair of hydroxy oxygens for $A_2B_{12}A_2$ at T_{SIM} = 430 K.

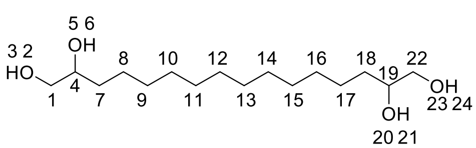

O_i	O_j	fraction	H-bond type
2	2	0.072	pri-pri
2	5	0.062	pri-sec
2	20	0.060	pri-sec
2	23	0.077	pri-pri
5	2	0.061	pri-sec
5	5	0.053	sec-sec
5	20	0.050	sec-sec
5	23	0.064	pri-sec
20	2	0.060	pri-sec
20	5	0.050	sec-sec
20	20	0.043	sec-sec
20	23	0.065	pri-sec
23	2	0.078	pri-pri
23	5	0.065	pri-sec
23	20	0.065	pri-sec
23	23	0.075	pri-pri

Supplementary Figures

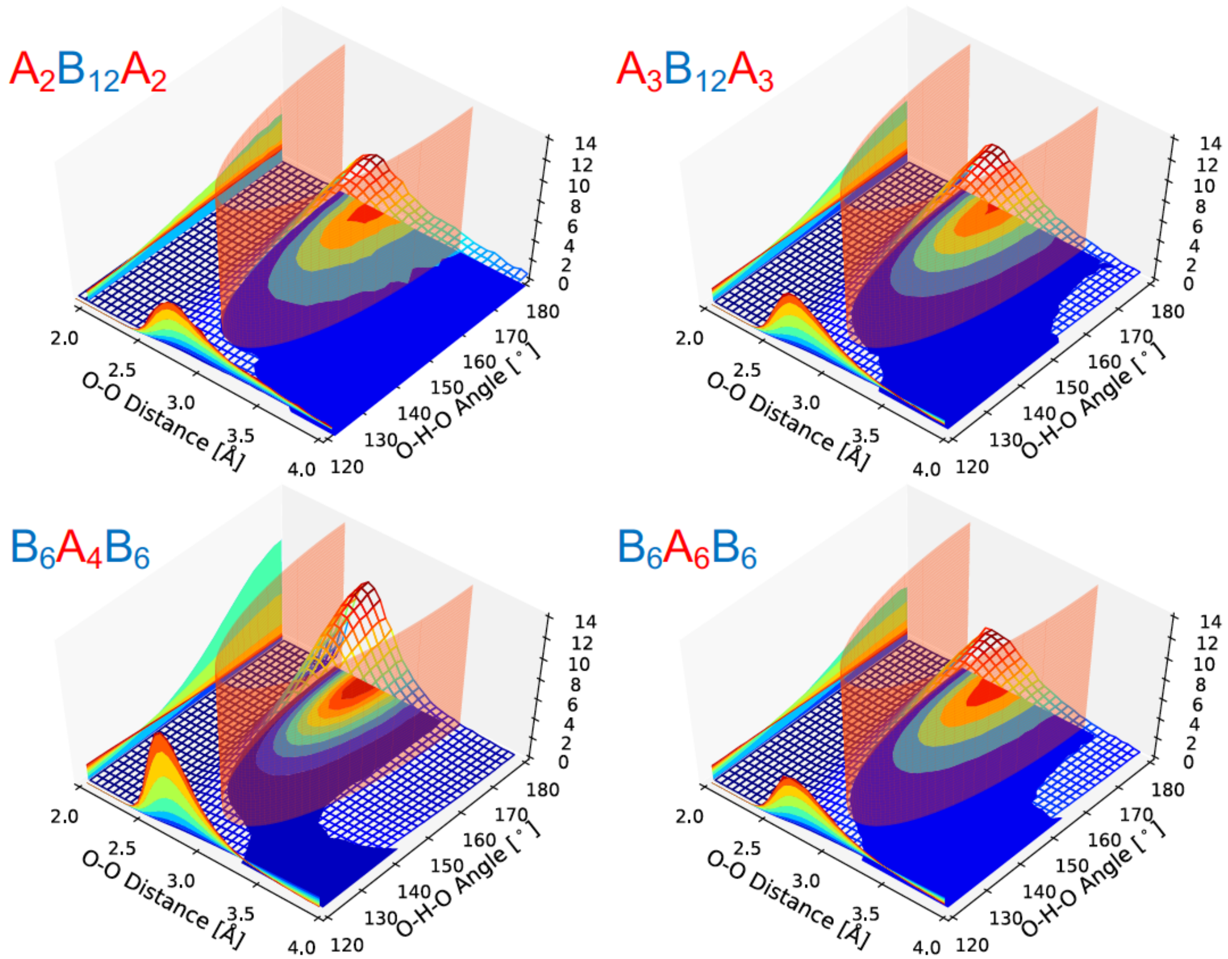

Figure S1. Radial-angular distribution functions (RADFs) for hydroxy groups of $A_2B_{12}A_2$, $A_3B_{12}A_3$, $B_6A_4B_6$, and $B_6A_6B_6$ amphiphiles at their lowest T_{SIM} above $T_{SIM,ODT}$. The radial and angular distributions are shown as 2-D projections of the RADF surfaces on vertical panes. The resulting RADF is normalized by a random distribution, with the Jacobian matrix corrected in the angular direction.

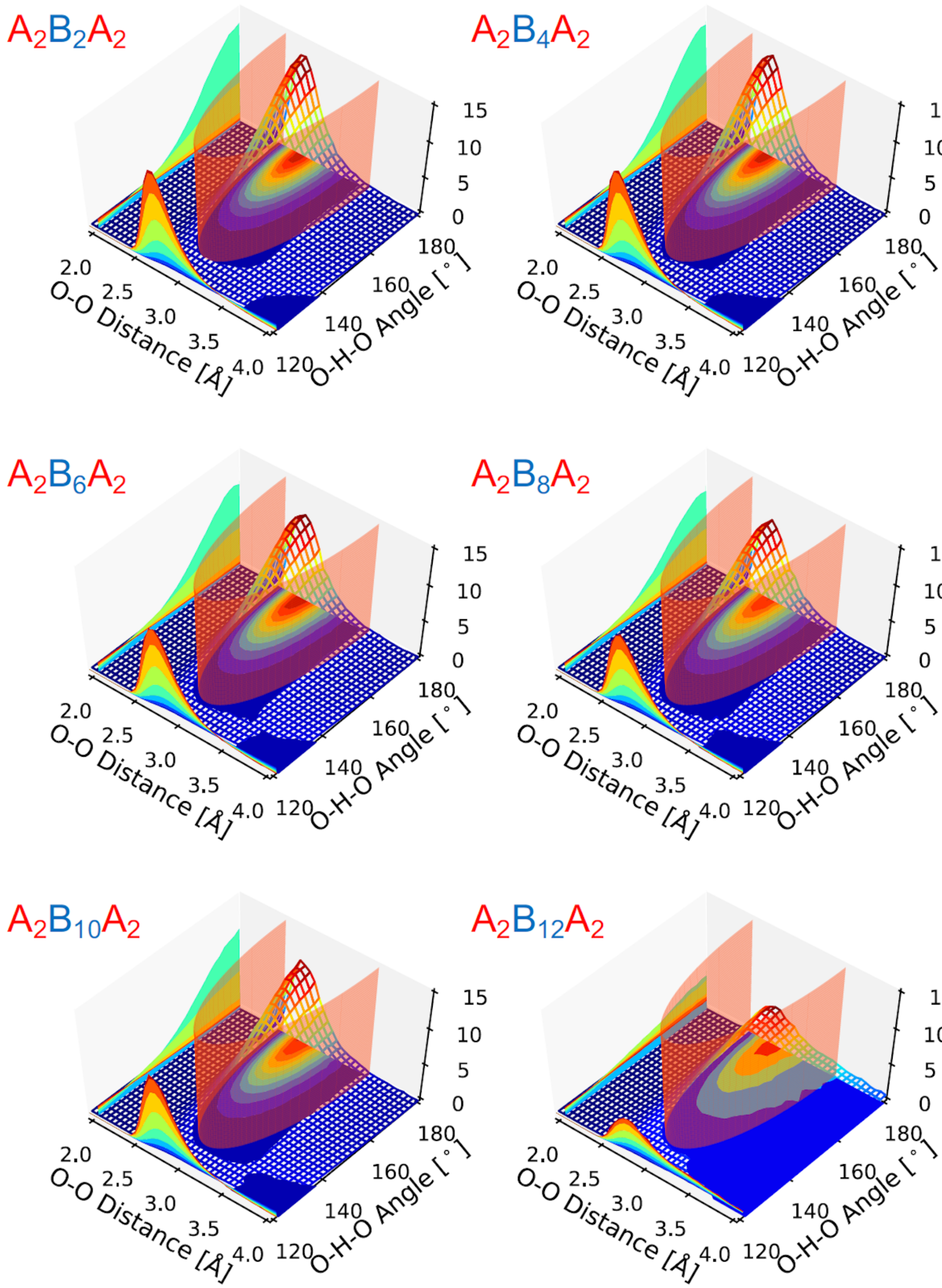

Figure S2. Radial-angular distribution functions (RADFs) for hydroxy groups of $A_2B_xA_2$ bola-amphiphiles at their lowest T_{SIM} above $T_{SIM,ODT}$. The radial and angular distributions are shown as 2-D projections of the RADF surfaces on vertical panes. The resulting RADF is normalized by a random distribution, with the Jacobian matrix corrected in the angular direction.

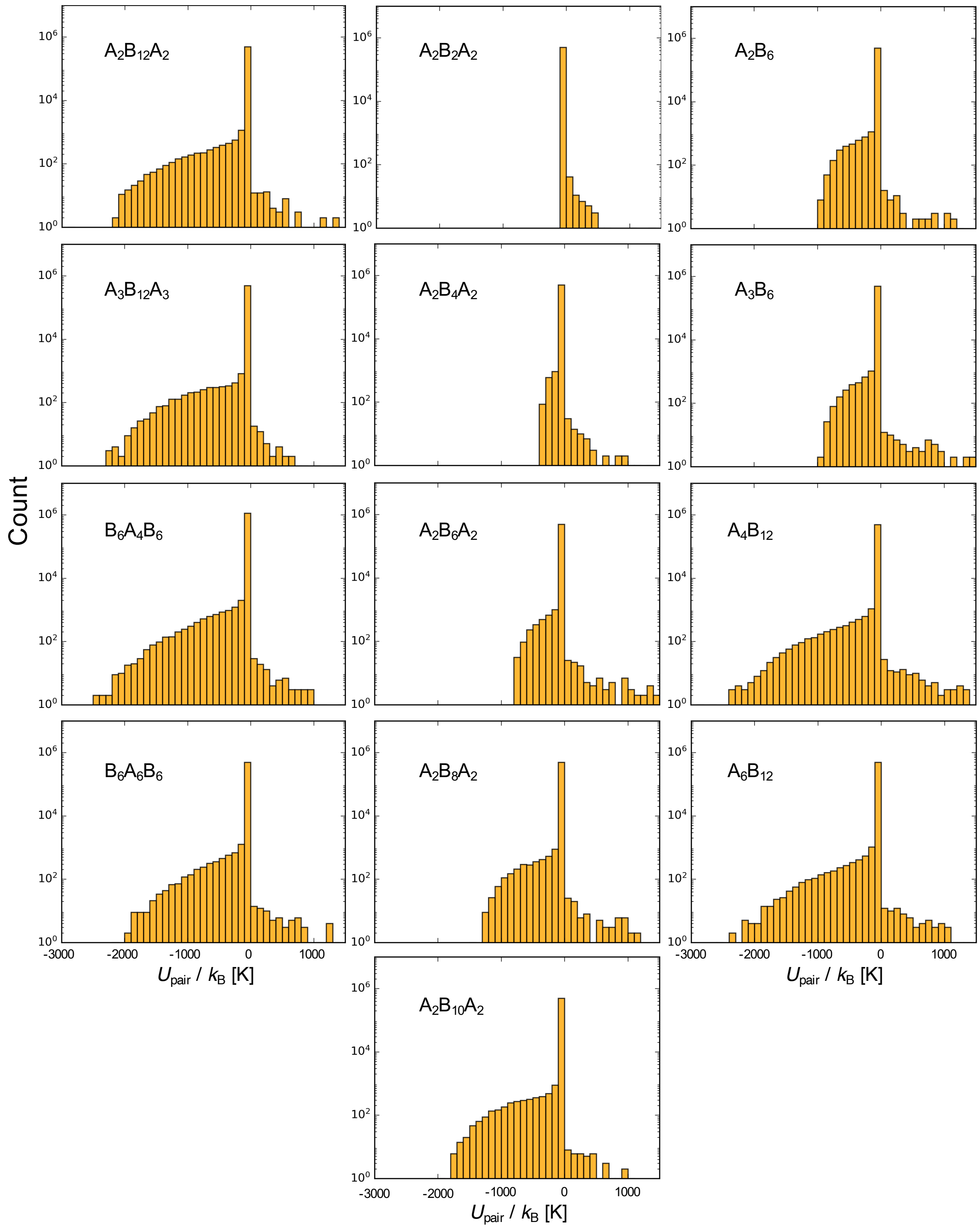

Figure S3. Histograms of the sum of intermolecular CH_q-CH_q Lennard-Jones interaction energies between the nonpolar parts (B blocks) for a pair of molecules in the DIS state obtained for ABA and BAB triblock and AB diblock amphiphiles. For example, the sum consists of 144 site-site energies for a pair of $B_6A_6B_6$ molecules containing each 12 CH_q units and accounts for the difference in the well depths of CH_3 and CH_2 units. The peak at $U_{pair} / k_B \approx 0$ K corresponds to spatially well separated molecules. The small fraction of molecules with $U_{pair} / k_B > 0$ K corresponds to molecules in close contact. The slope in these histograms is relatively small at $U_{pair} / k_B = -T$.

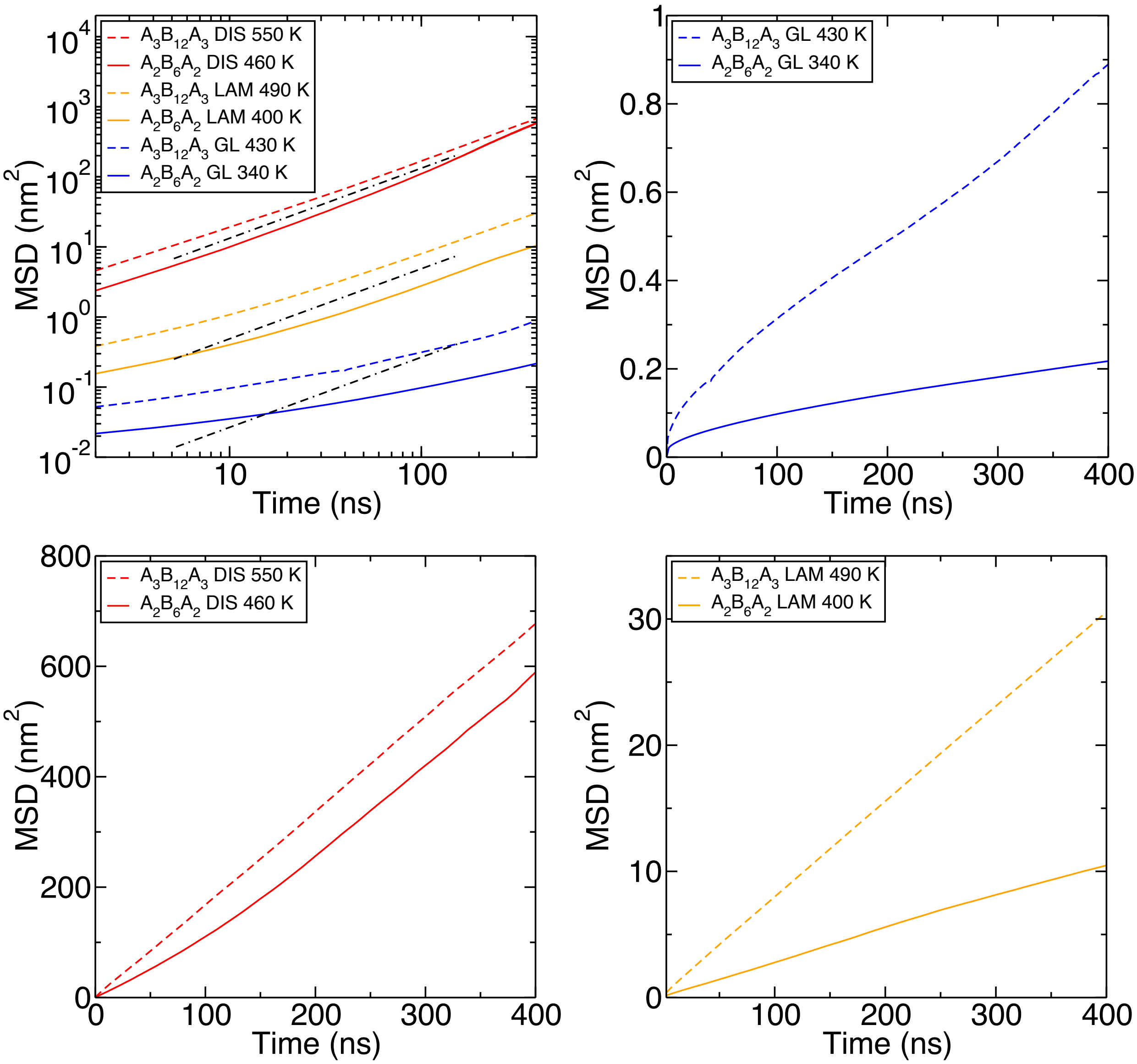

Figure S4. Mean square displacements (MSDs) in log-log and linear-linear scales for $A_3B_{12}A_3$ and $A_2B_6A_2$ molecules at temperatures yielding GL, LAM, and DIS morphologies. These two compounds are at the low- and high-end of the molecular weight range for ABA triblock amphiphiles investigated here. Data are shown for the final 400 ns of the trajectories because molecules are sometimes more mobile during the initial phase of trajectory that is started from a highly-disordered structure. In the log-log plot, the dash-dotted black lines show a slope of unity. Over a 100 ns interval, the MSDs for the GL and DIS phases are significantly smaller and larger, respectively, than d^2 observed for the LAM phase (where d is the domain spacing).

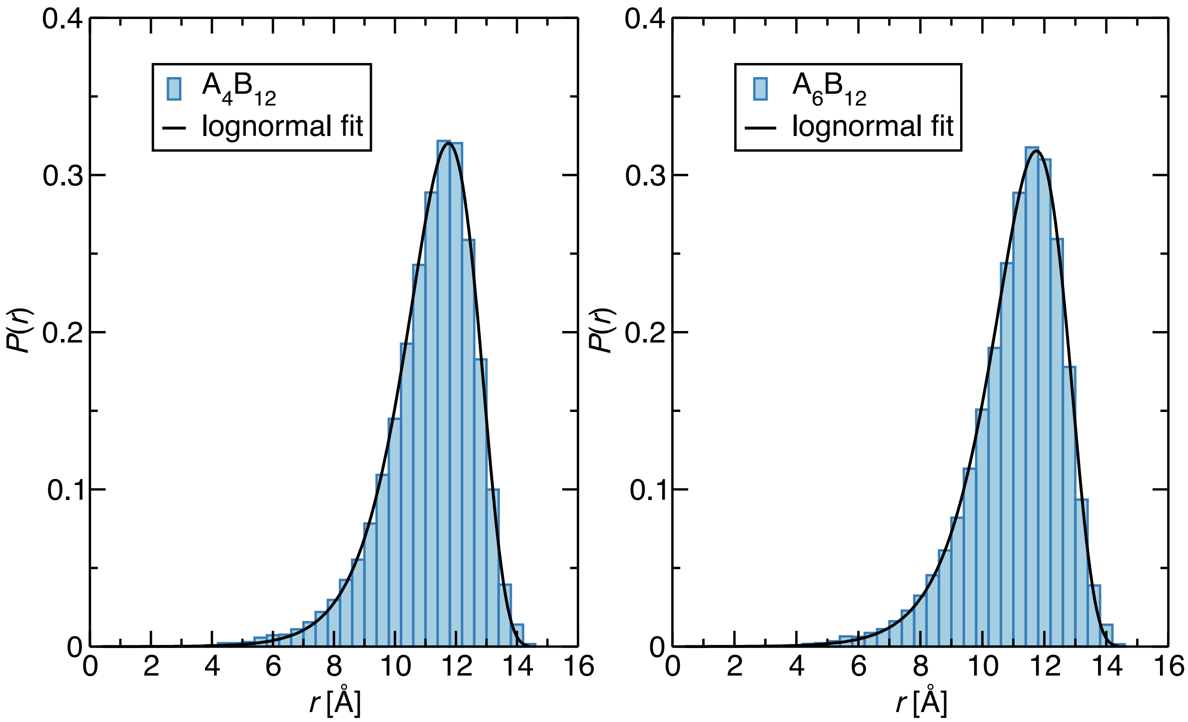

Figure S5. Probability distributions of the end-to-end lengths of the alkyl tails for A_4B_{12} and A_6B_{12} diblock amphiphiles at T_{SIM} = 520 K. The average lengths are 11.2 and 11.1 Å for A_4B_{12} and A_6B_{12}, respectively.

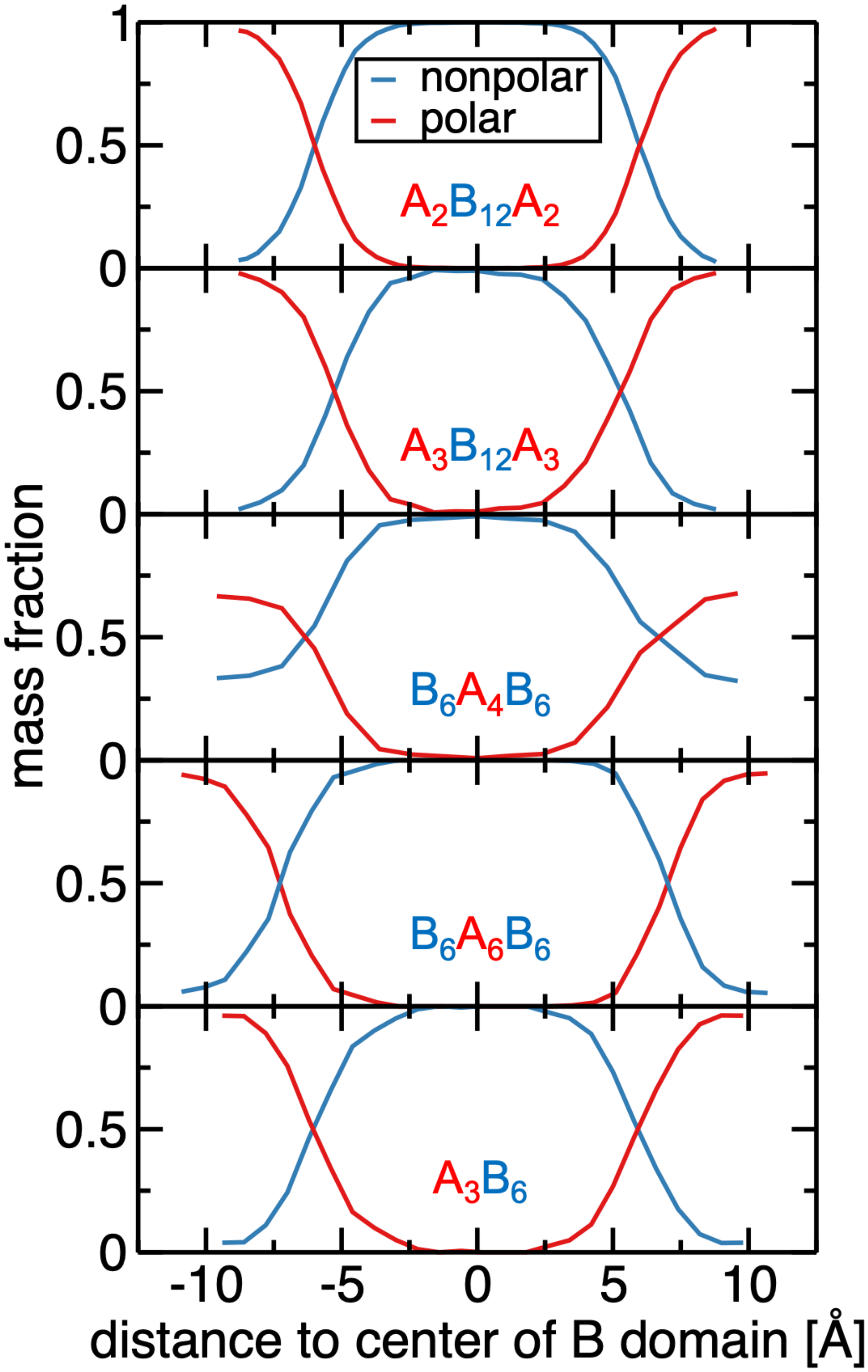

Figure S6. Composition profiles along the normal of the lamellar planes for $A_2B_{12}A_2$ at T_{SIM} = 460 K, $A_3B_{12}A_3$ at 460 K, $B_6A_4B_6$ at 440 K, $B_6A_6B_6$ at 520 K, and A_3B_6 at 430 K. Polar and nonpolar mass fractions are shown red and blue, respectively.

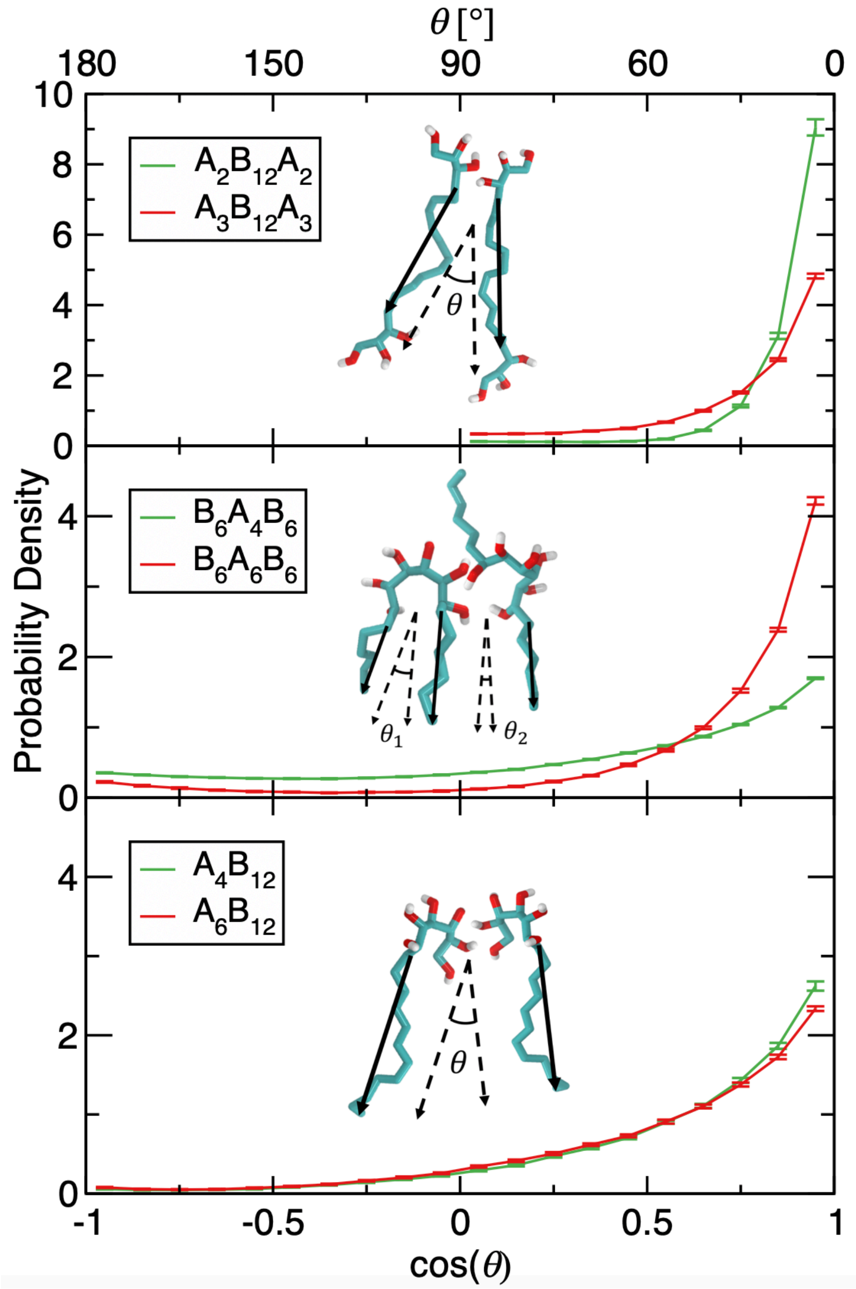

Figure S7. Angular distributions of the end-to-end vectors of neighboring B blocks for (top) the LAM phases of ABA amphiphiles, (middle) the PL and HPL phases of BAB amphiphiles, and (bottom) the LAM phases of AB amphiphiles. The schematics are drawn to guide the eye. Two B blocks are considered as neighbors when their center-of-mass distance is less than or equal to 8 Å, consistent with the neighbor definition in Chen *et al*.[8] The angle between two neighboring ABA amphiphile can only range from 0 to 90°.

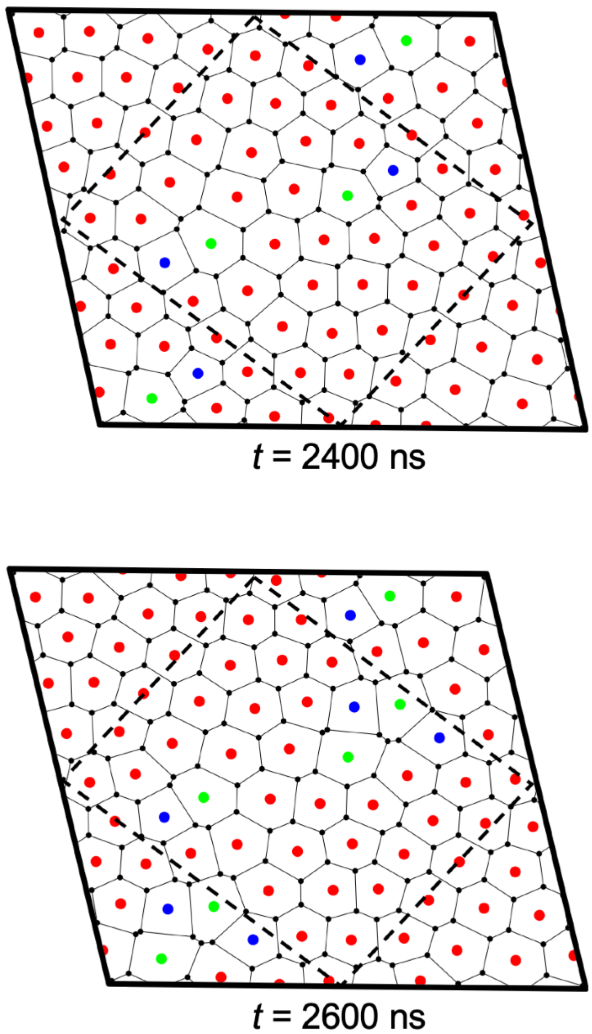

Figure S8. Voronoi tessellation of one perforated layer for the $B_6A_4B_6$ amphiphile at T_{SIM} = 440 K at different times during the trajectory. The parallelogram-shaped frame contains two repeat units (indicated by the dashed lines). The blue, red, and green dots indicate pentagons, hexagons, and heptagons, respectively.

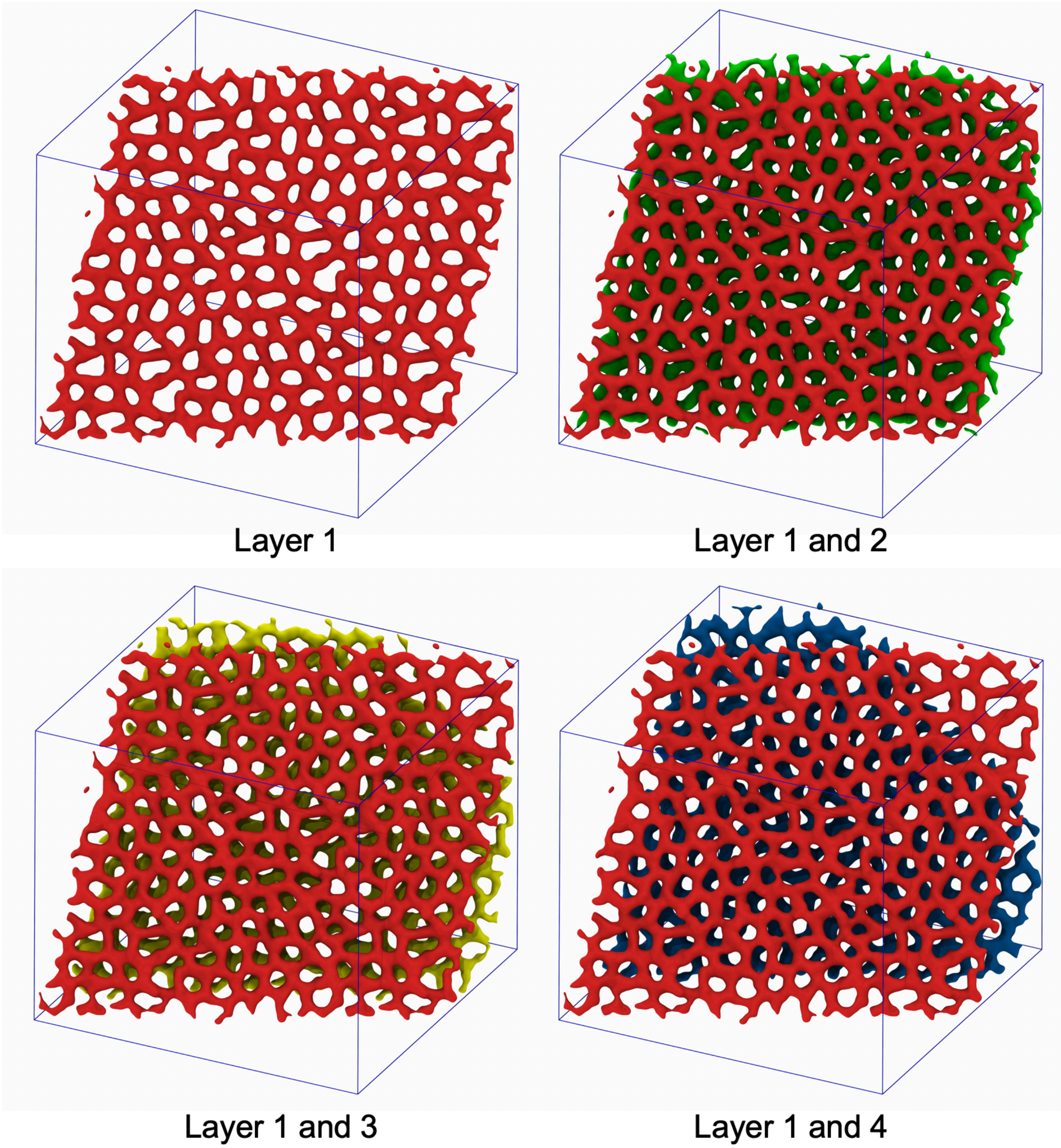

Figure S9. Perpendicular views from the reference layer (Layer 1) in the $B_6A_4B_6$ system at T_{SIM} = 440 K. To access more details of the perforations, the box is replicated three times in each dimension using periodic images.

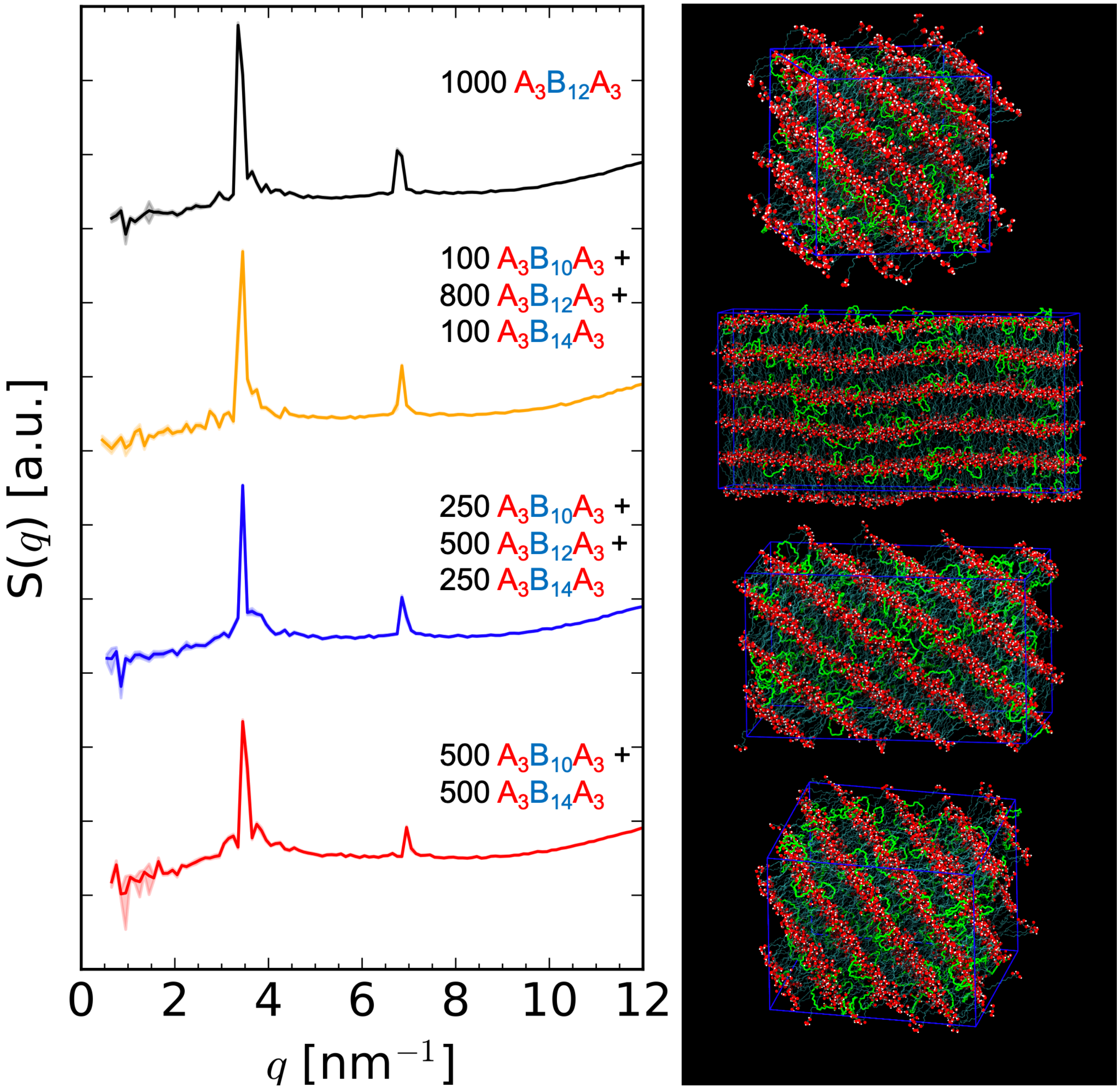

Figure S10. Structure factors and simulation snapshots for $A_3B_{12}A_3$ amphiphiles and $A_3B_{10}A_3$/$A_3B_{12}A_3$/$A_3B_{14}A_3$ mixtures at T_{SIM} = 490 K; "loops" are highlighted in green and "bridges" are shown with transparent alkyl chains.

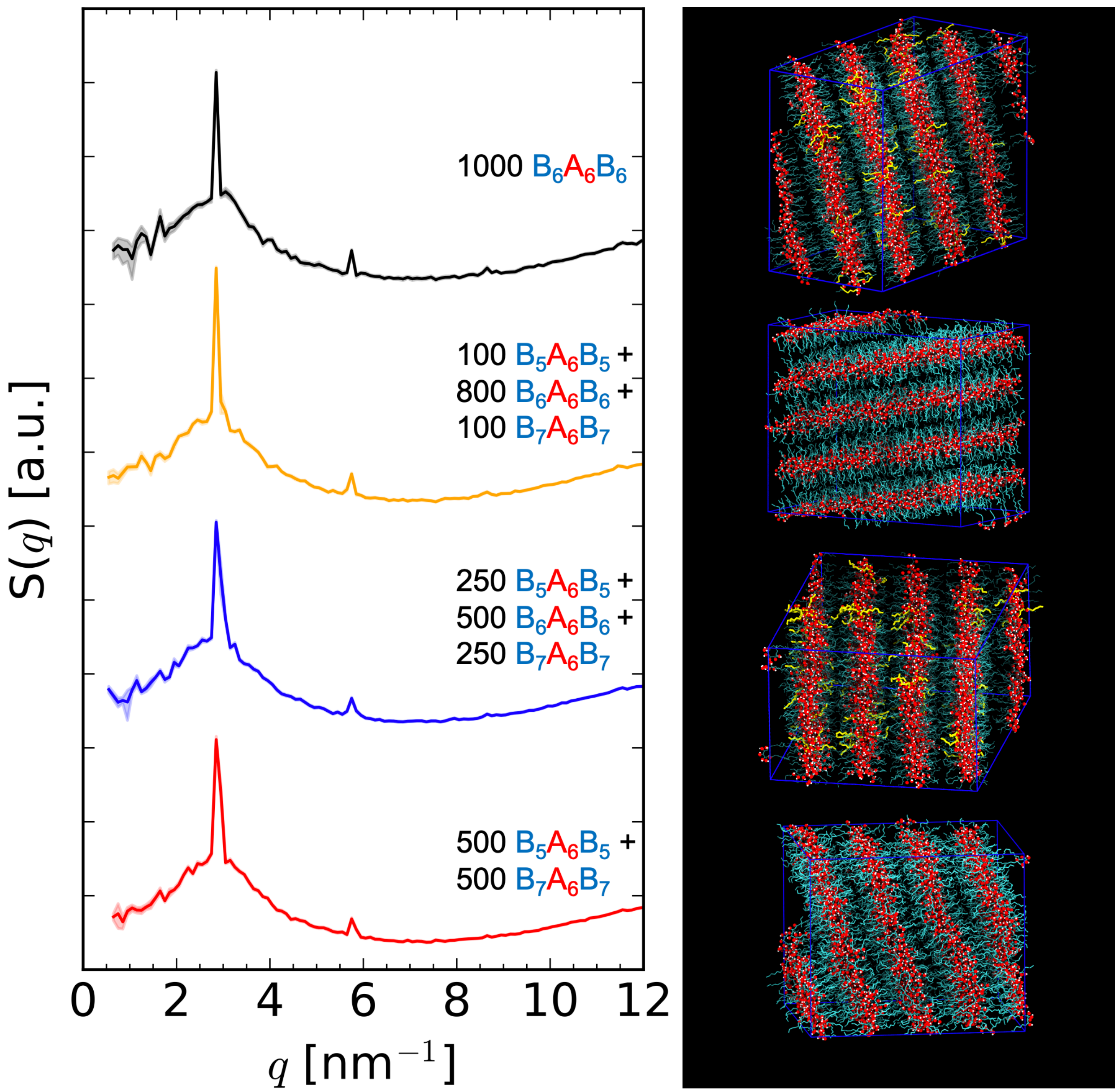

Figure S11. Structure factors and simulation snapshots for $B_6A_6B_6$ amphiphiles and $B_5A_6B_5$/$B_6A_6B_6$/$B_7A_6B_7$ mixtures at T_{SIM} = 520 K. For neat $B_6A_6B_6$ and the 1:2:1 mixture, alkyl chains connected by polar "bridges" are highlighted in yellow and those connected by polar "loops" are shown as transparent.

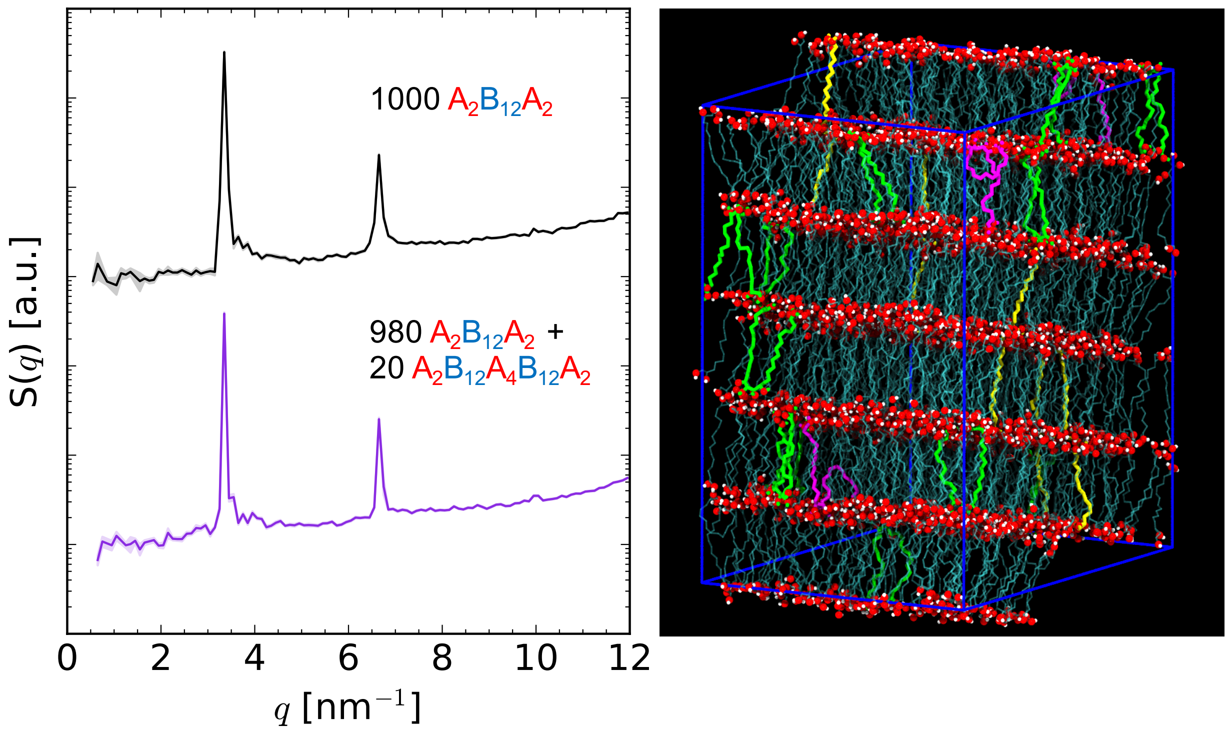

Figure S12. Left: structure factors for $A_2B_{12}A_2$ amphiphiles (N = 1000) and the mixture of $A_2B_{12}A_2$ triblock (N = 980) and $A_2B_{12}A_4B_{12}A_2$ pentablock (N = 20) at T_{SIM} = 430 K. Right: simulation snapshot of the $A_2B_{12}A_2$/$A_2B_{12}A_4B_{12}A_2$ mixture, with all of the pentablocks highlighted. Conformations include “bridge-bridge” in the same domain (green), “bridge-bridge” spanning two domains (yellow), and “bridge-loop” (magenta).

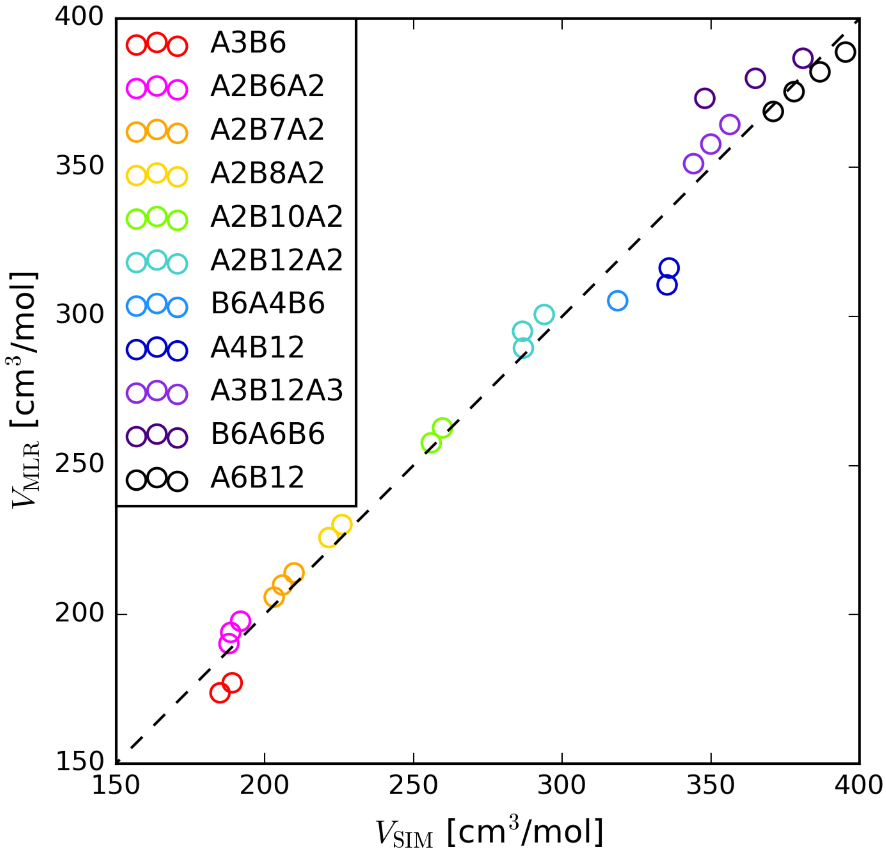

Figure S13. Molar volumes of ordered phases obtained for ABA, BAB, and AB amphiphiles versus molar volumes predicted by multiple-linear regression using the equation:

$$V_{\mathrm{MLR}} = \left(n_{\mathrm{CH_2OH}}V_{\mathrm{CH_2OH}} + n_{\mathrm{CHOH}}V_{\mathrm{CHOH}} + n_{\mathrm{CH_3}}V_{\mathrm{CH_3}} + n_{\mathrm{CH_2}}V_{\mathrm{CH_2}}\right)\left(1 + \alpha(T_{\mathrm{SIM}} - 370)\right)$$

The fitting coefficients are: $V_{\mathrm{CH_2OH}} = 24.4\ \mathrm{cm^3/mol}$, $V_{\mathrm{CHOH}} = 23.9\mathrm{cm^3/mol}$, $V_{\mathrm{CH_3}} = 20.1\ \mathrm{cm^3/mol}$, $V_{\mathrm{CH_2}} = 15.6\mathrm{cm^3/mol}$, and $\alpha = 0.00066\ \mathrm{K^{-1}}$.

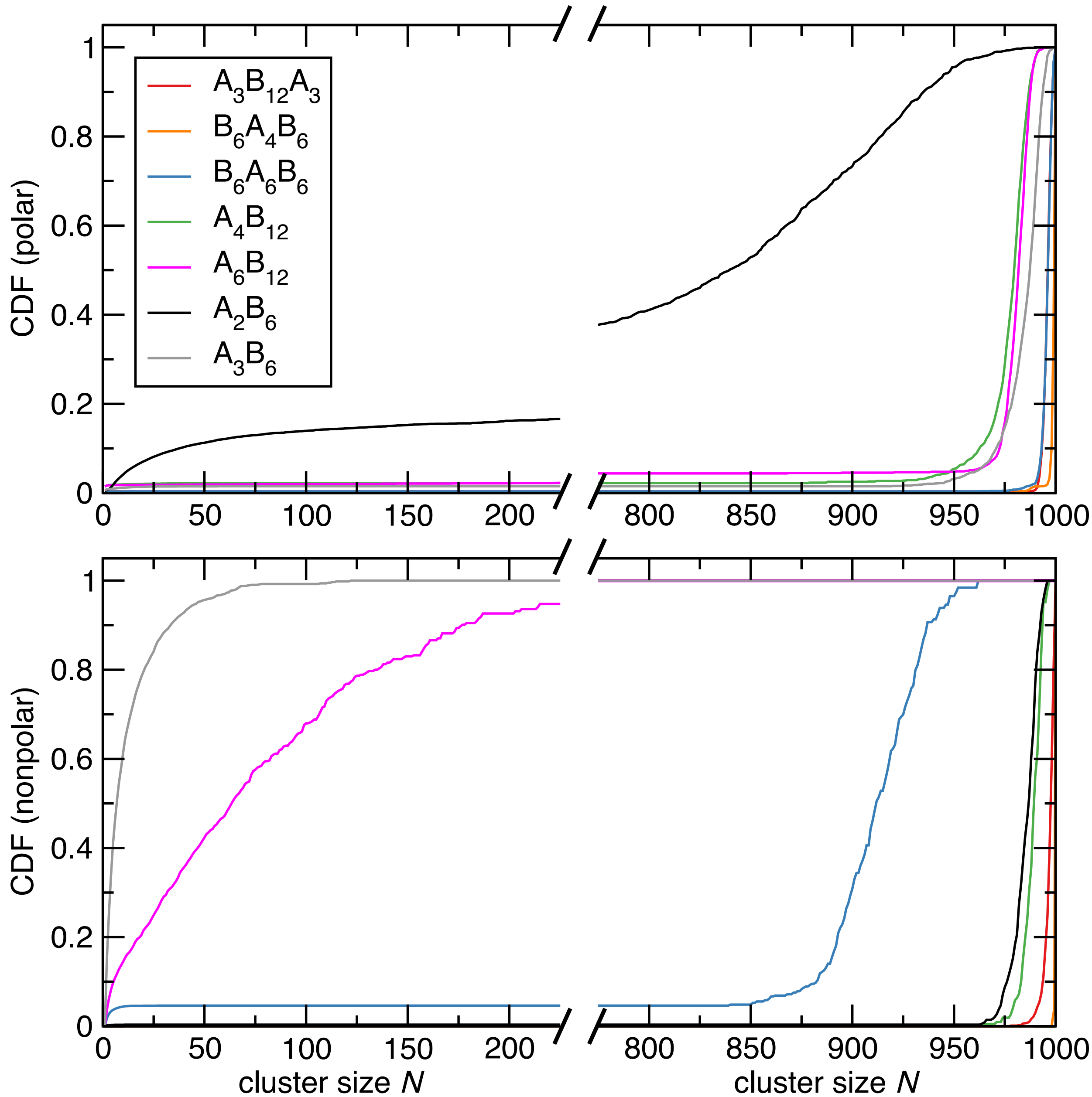

Figure S14. Cumulative distribution functions for the probability of finding $A_3B_{12}A_3$, $B_6A_4B_6$, and $B_6A_6B_6$ triblock amphiphiles and A_xB_y diblock amphiphiles in a hydrogen-bonded (top) and nonpolar (bottom) aggregate of size of N for the disordered phases near T_{ODT}. For $B_6A_4B_6$, N is scaled by 1000/1504 to account for the different number of molecules.

References

(1) Martin, M. G.; Siepmann, J. I. Transferable Potentials for Phase Equilibria. 1. United-Atom Description of n-Alkanes. *J. Phys. Chem. B* **1998**, *102*, 2569–2577.

(2) Martin, M. G.; Siepmann, J. I. Novel Configurational-Bias Monte Carlo Method for Branched Molecules. Transferable Potentials for Phase Equilibria. 2. United-Atom Description of Branched Alkanes. *J. Phys. Chem. B* **1999**, *103*, 4508–4517.

(3) Chen, B.; Potoff, J. J.; Siepmann, J. I. Monte Carlo Calculations for Alcohols and Their Mixtures with Alkanes. Transferable Potentials for Phase Equilibria. 5. United-Atom Description of Primary, Secondary, and Tertiary Alcohols. *J. Phys. Chem. B* **2002**, *105*, 3093–3104.

(4) Stubbs, J. M.; Potoff, J. J.; Siepmann, J. I. Transferable Potentials for Phase Equilibria. 6. United-Atom Description for Ethers, Glycols, Ketones, and Aldehydes. *J. Phys. Chem. B* **2004**, *108*, 17596–17605.

(5) Jorgensen, W. L.; Maxwell, D. S.; Tirado-Rives, J. Development and Testing of the OPLS All-Atom Force Field on Conformational Energetics and Properties of Organic Liquids. *J. Am. Chem. Soc.* **1996**, *118*, 11225–11236.

(6) Hess, B. P-LINCS: A Parallel Linear Constraint Solver for Molecular Simulation. *J. Chem. Theory Comput.* **2008**, *4*, 116–122.

(7) Brown, P. J.; Fox, A. G.; Maslen, E. N.; O'Keefe, M. A.; Wills, T. M. *International Tables for Crystallography*, Prince, E.; International Union of Crystallography: Dordrecht, The Netherlands, 2004; Vol. C.

(8) Chen, Q. P.; Barreda, L.; Oquendo, L. E.; Hillmyer, M. A.; Lodge, T. P.; Siepmann, J. I. Computational Design of High-χ Block Oligomers for Accessing 1 nm Domains. *ACS Nano* **2018**, *12*, 4351–4361.